Science Advances
AAAS

advances.sciencemag.org/cgi/content/full/6/31/eaba8761/DC1

Supplementary Materials for

On-demand spin-state manipulation of single-photon emission from quantum dot integrated with metasurface

Yanjun Bao, Qiaoling Lin, Rongbin Su, Zhang-Kai Zhou, Jindong Song, Juntao Li*, Xue-Hua Wang*

*Corresponding author. Email: lijt3@mail.sysu.edu.cn (J.L.); wangxueh@mail.sysu.edu.cn (X.-H.W.)

Published 29 July 2020, *Sci. Adv.* **6**, eaba8761 (2020)
DOI: 10.1126/sciadv.aba8761

This PDF file includes:

Supplementary Text

Design of metasurface for manipulating QD emission

In our designed structure, the quantum dot (QD) is placed in a dielectric layer, with a metallic mirror at the bottom to reflect the QD emission and a layer of metasurface at the top for manipulating the QD emission (Figure S1a). The metasurface can feel the QD emission from two paths, one is the directly emitted from the QD (red arrow), and the other is the emission reflected by the metallic mirror (blue arrow). For the reflection path, it can be considered as the emission from the mirror image of the QD, which is located at a distance of 2*l* from the original QD (*l* is the distance of the QD to the metallic mirror). Considering the QD as a dipole, if it rotates anti-clockwise, the mirror image of QD also rotates anti-clockwise, but with a π phase difference with the original QD (Figure S1b). Therefore, the polarizations of the QD emissions from the two paths are the same.

For the LCP of the QD emission, the metasurface element (Si nanoblock) with an in-plane rotation angle φ and a distance of *r* from the center *O* can alter the LCP to RCP with a Pancharatnam−Berry (PB) phase of -2φ. Then the RCP light passing through the metasurface can be written as

$$E_R = \frac{\cos(\gamma_1)}{r_1}\exp[i(2\pi n r_1/\lambda - 2\varphi)] + \frac{\cos(\gamma_2)}{r_2}\exp[i(2\pi n r_2/\lambda - 2\varphi + \pi)] \quad \text{(S1)}$$

where the first and second terms represent the electric fields from the directly QD emission and the one reflected by the metallic mirror, r_1 (r_2) is the distance between the original QD (mirror QD image) and the metasurface element, γ_1(γ_2) is the angle between r_1 (r_2) and the vertical dashed line, λ is the wavelength of the QD emission and *n* is the refractive index of dielectric layer. If the QD emission can be converted by metasurface into a beam along the direction with an angle of θ_1 relative to *x* axis in *xz* plane, we have

$$\arg(E_R) = k_0 \sin(\theta_1) x + 2p\pi \quad \text{(S2)}$$

where arg is argument of a complex number, k_0 ($2\pi/\lambda$) is the wavevector in air, *x* is the *x* coordinate of the metasurface element and *p* is an integer.

For the RCP of the QD emission, the metasurface element can alter the RCP to LCP with a PB phase of +2φ. Then the LCP light passing through the metasurface can be written as

$$E_L = \frac{\cos(\gamma_1)}{r_1}\exp[i(2\pi n r_1/\lambda + 2\varphi)] + \frac{\cos(\gamma_2)}{r_2}\exp[i(2\pi n r_2/\lambda + 2\varphi + \pi)] \quad \text{(S3)}$$

If the LCP QD emission can be converted into a beam along the direction with an angle of θ_2 relative to x axis in xz plane, we have

$$\arg(E_L) = k_0 \sin(\theta_2)x + 2q\pi \tag{S4}$$

where q is an integer. Therefore, the metasurface can control the QD emission and converted it into LCP beam along the direction of angle θ_1 and RCP beam along the direction of angle θ_2. The positions (x,y) and its corresponding orientation angle φ of the Si nanoblock in the metasurface can be determined by the simultaneous equation of (S2) and (S4), as

$$\begin{cases} -2\varphi + \arg\left[\dfrac{\cos(\gamma_1)}{r_1}\exp(i2\pi n r_1/\lambda) - \dfrac{\cos(\gamma_2)}{r_2}\exp(i2\pi n r_2/\lambda)\right] = 2\pi\sin(\theta_1)x/\lambda + 2p\pi \\ +2\varphi + \arg\left[\dfrac{\cos(\gamma_1)}{r_1}\exp(i2\pi n r_1/\lambda) - \dfrac{\cos(\gamma_2)}{r_2}\exp(i2\pi n r_2/\lambda)\right] = 2\pi\sin(\theta_2)x/\lambda + 2q\pi \end{cases} \tag{S5}$$

By inserting the parameters of θ_1, θ_2, h, l, λ and n, the positions (x,y) and corresponding orientation angle φ of each nanoblock can be totally determined. Figure S2b shows a top view of a typical metasurface with parameters of θ_1=10°, θ_2=-10°, h=2 μm, l=1 μm, λ=910 nm and n=1.45. The diameter of the metasurface is 12 μm.

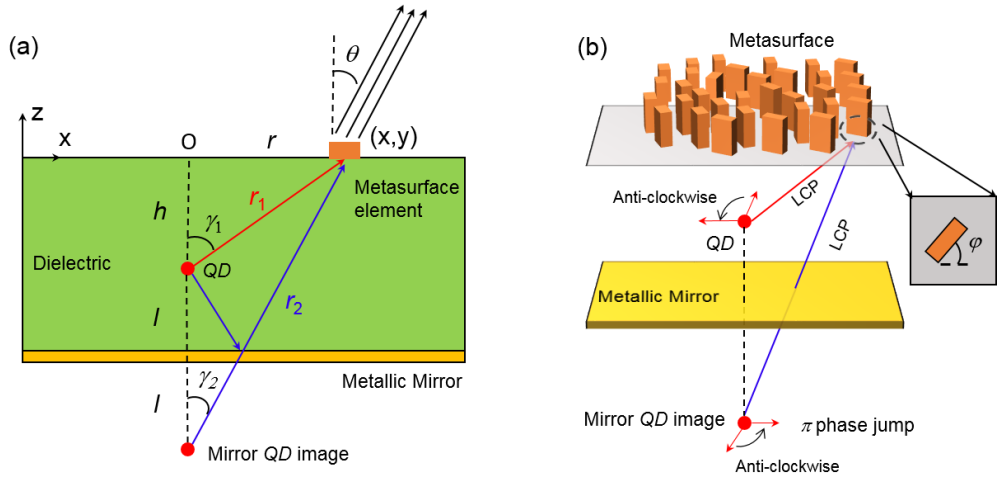

Fig. S1. Schematic view of the metasurface and QD. (a-b) Side (a) and 3D (b) views of the designed device consisting of a layer of dielectric that is sandwiched between gold mirror and a silicon metasurface. The QD is embedded in the dielectric layer. The QD emission reflected by the gold mirror can be considered as the one from a mirror QD image that locates below the gold mirror. The relations of the phases and polarizations between the original and mirror QD images are indicated in (b).

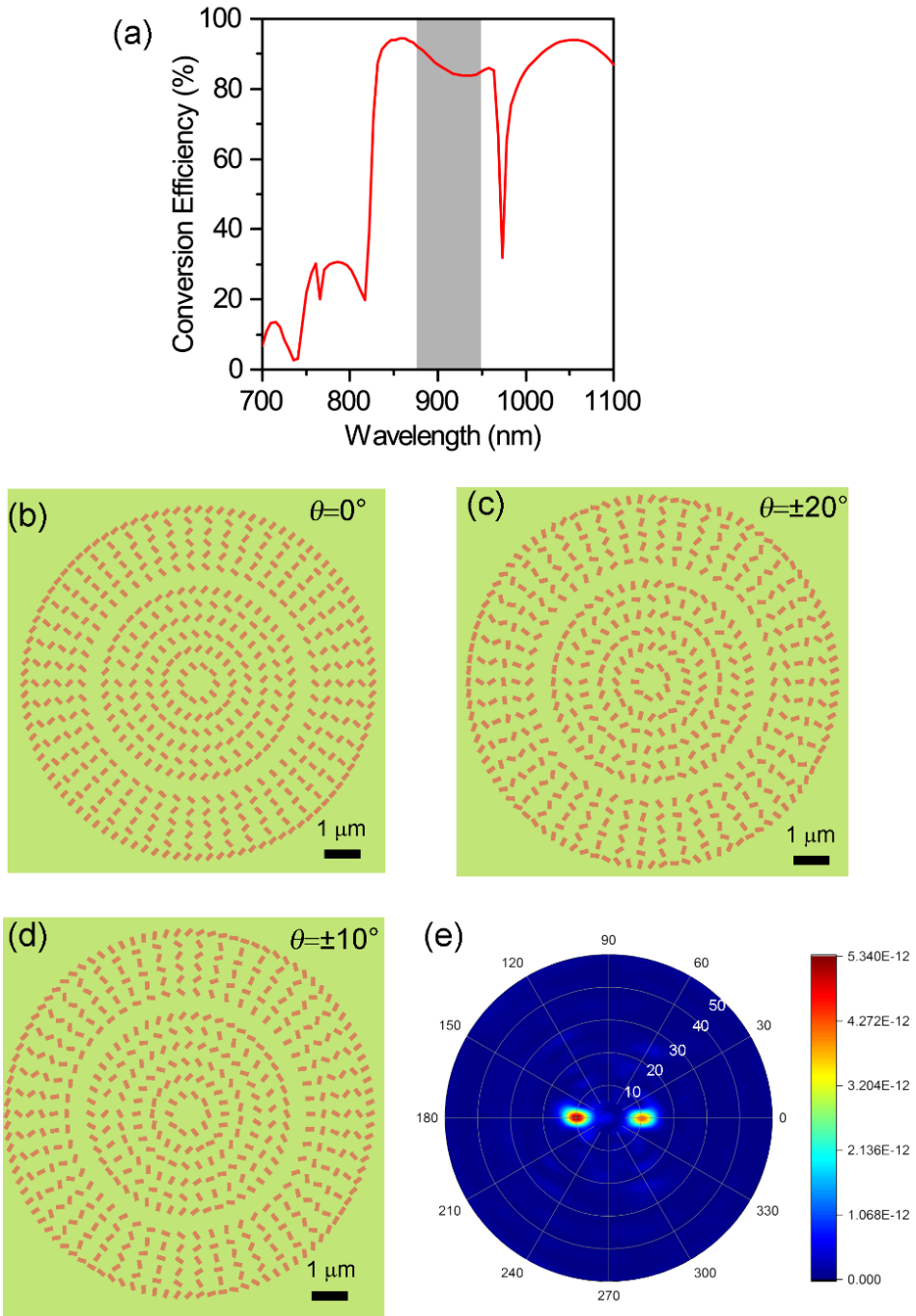

Fig. S2. Simulated polarization conversion of a Si nanoblock, the top views of Si metasurface with designed θ=0°and θ=±20° and the simulation results of another case with θ=±10°. (a) The calculated polarization conversion efficiency of an optimized Si nanoblock as a function of wavelength. The geometry of Si nanoblock is optimized over a broadband wavelength 880-950 nm for high conversion efficiency with width 140 nm, length 280 nm and height 600 nm. In the simulation, the structure consists of Si nanoblock units on SiO_2 substrate with a period of 450 nm. Circularly polarized light is illuminated from the substrate side. If only optimized at 910 nm, the

conversion efficiency can reach up to 97% for a Si nanoblock with 245 nm length, 86 nm width and 600 nm height. The gray rectangle region indicates the wavelength range of 880-950 nm. (b-c) The top view of designed metasurfaces in figure 2 in the main text for manipulating QD emission with θ=0° (b) and θ=±20° (c). (d) The top view of a designed metasurface for manipulating QD emission. The parameters are θ_1=10°, θ_2=-10°, h=2 μm, l=1 μm, λ=910 nm and n=1.45. (e) The simulated far-field scattering pattern. The two beams are propagating along the directions exactly at our designed angels of ±10°.

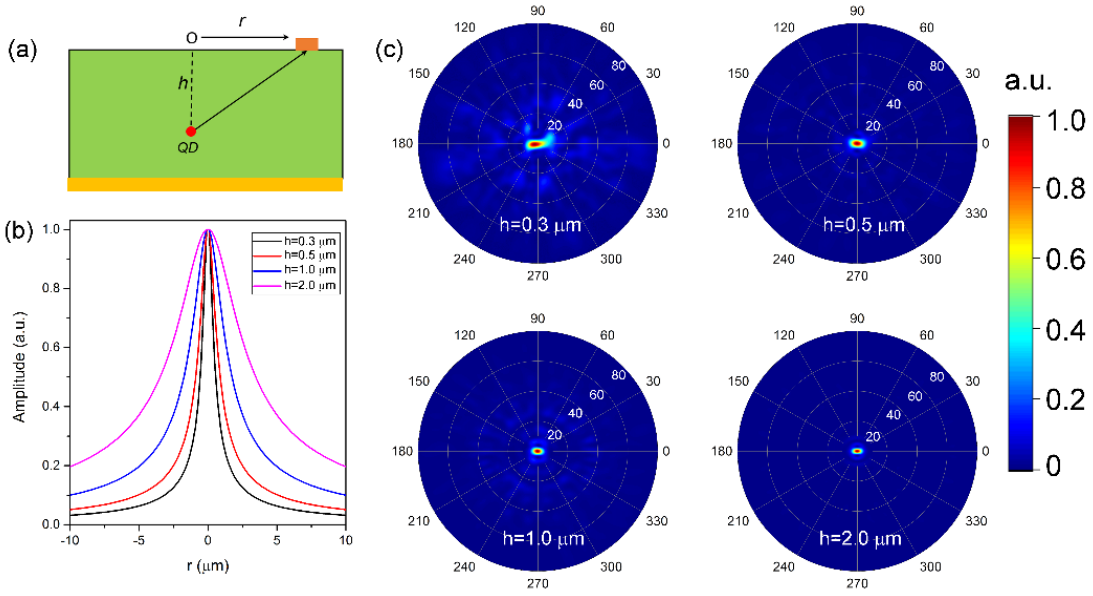

Fig. S3. Device performance dependence on the distance from the QD to metasurface. (a) Schematic of the relative positions between the QD and metasurface. (b) The amplitude of QD emission at different positions of metasurface for h =0.3 μm, 0.5 μm, 1μm and 2 μm. The amplitude of light that illuminates on the metasurface is not homogeneous, but follows as $(r^2+h^2)^{-1/2}$. For smaller h value, the amplitude decays rapidly, which means that only a small effect area can contribute to the beam formation. With the increasing of h, the amplitude decay slowly, indicating a much larger effect area for beam generation. (c) The simulated far-field scattered patterns for the structures with the four different h, with the values indicated in each panel. One can see that the divergent angle of the center bright spot and the stray scatterings along other directions decrease with the increasing of h.

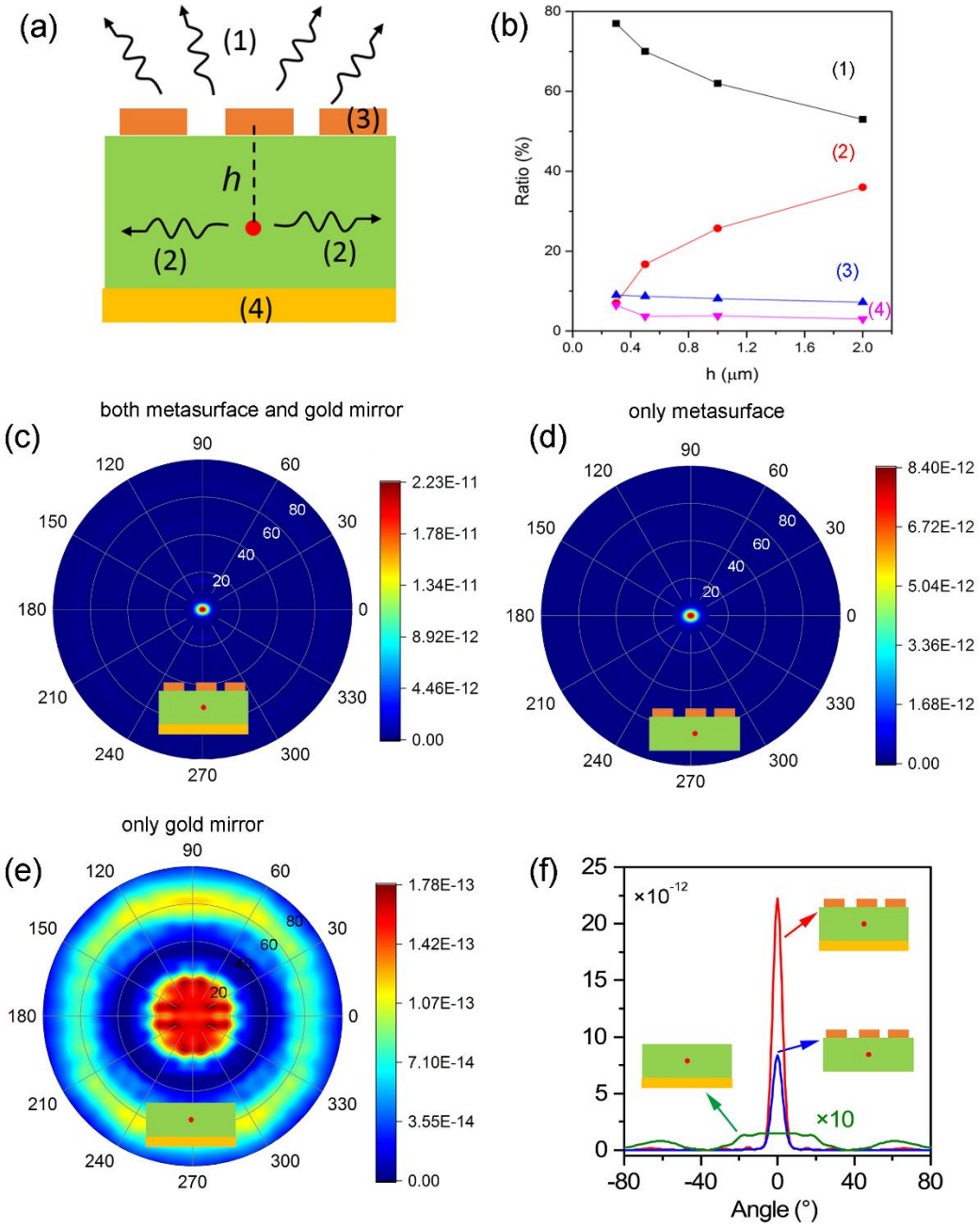

Fig. S4. Dissipation channels of the QD emissions and Simulated far-field patterns of the different QD-metasurface devices. (a) Schematics of the four dissipation channels of the QD emissions. The emitted energy of QD are dissipated via four channels: (1) the scattering upwards passing through metasurface; (2) the scattering along the dielectric layer; (3) the absorption by the metasurface and (4) the absorption by the gold mirror. The energy through the first channel is the one we need, and the ratio between it to the emitted energy by QD is defined as the collection efficiency. (b) The percentages of the energies of the four channels dependence on the *h* value. Because the absorptions by metasurface and gold mirror are mainly determined by the inherent dissipations of the materials, the energy losses through channels (3) and (4) almost have no changes. However, the energy through channel (1)

decreases and the one through channel (2) increases with the increasing of *h*. This can be understood as follows: with the increasing of *h,* the optical modes of the center dielectric layer increase, and therefore the leakage radiation through channel (2) increases. (c-e) Simulated far-field patterns of the QD devices with both the metasurface and gold mirror (c), only the top metasurface (d) and only the gold mirror (e). The insets show the side view of the structures. Without the metasurface structure, the QD emits light in a wide range of directions in the upper hemisphere. (f) Line plots of the far-field scattering intensity along horizontal direction for the above three structures. The intensity peak of structure in (c) is about two times of the one in (d).

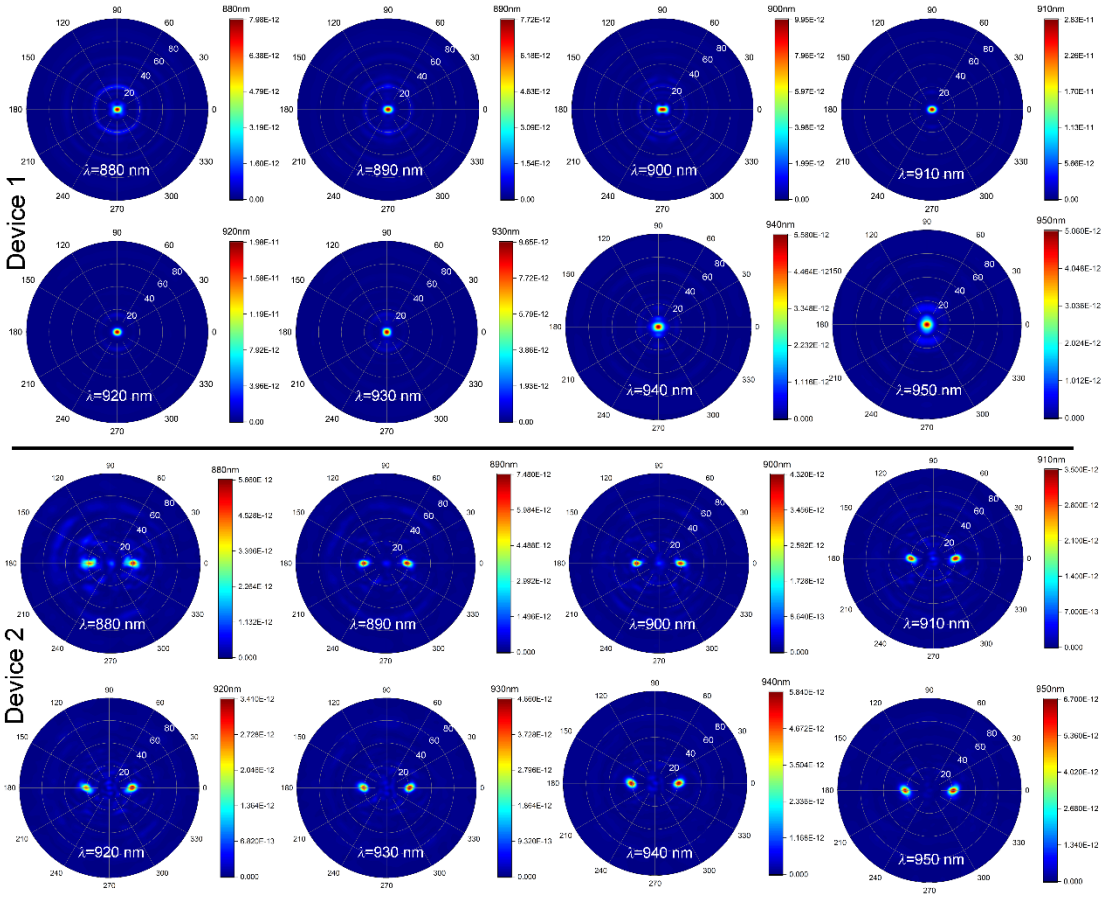

Fig. S5. Simulated far-field scattering patterns of the devices 1 and 2 operated at different wavelengths from 880 nm to 950 nm. Both devices are designed for 910 nm. The operation wavelengths are labeled at each panel. For device 2, the two spots in the far-field scattering patterns are obvious for all wavelegnths, with a slight deviation of the scattering angle from the designed ±20° at 910 nm.

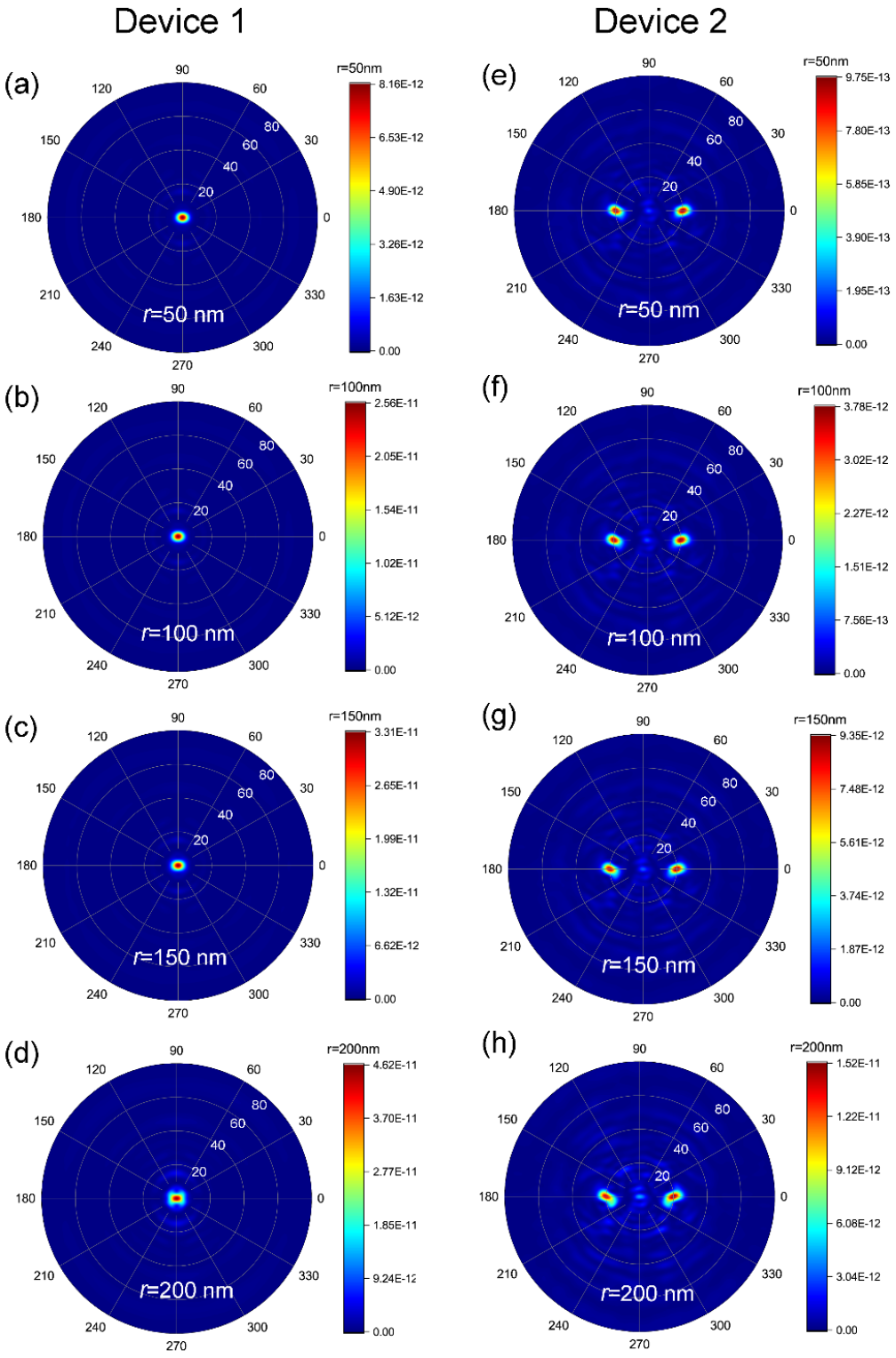

Fig. S6. Simulated far-field patterns of devices 1 (a-d) and 2 (e-h) with QD in GaAs nanopillar with different radius. (a-d) Simulated total far-field patterns of the device of θ=0° when the QD is in a GaAs nanopillar with radius of 50 nm (a), 100 nm (b), 150 nm (c) and 200 nm (d). (e-h) Simulated total far-field patterns of the device of θ=20° when the QD is in a GaAs nanopillar with radius of 50 nm (e), 100 nm (f), 150 nm (g) and 200 nm (h).

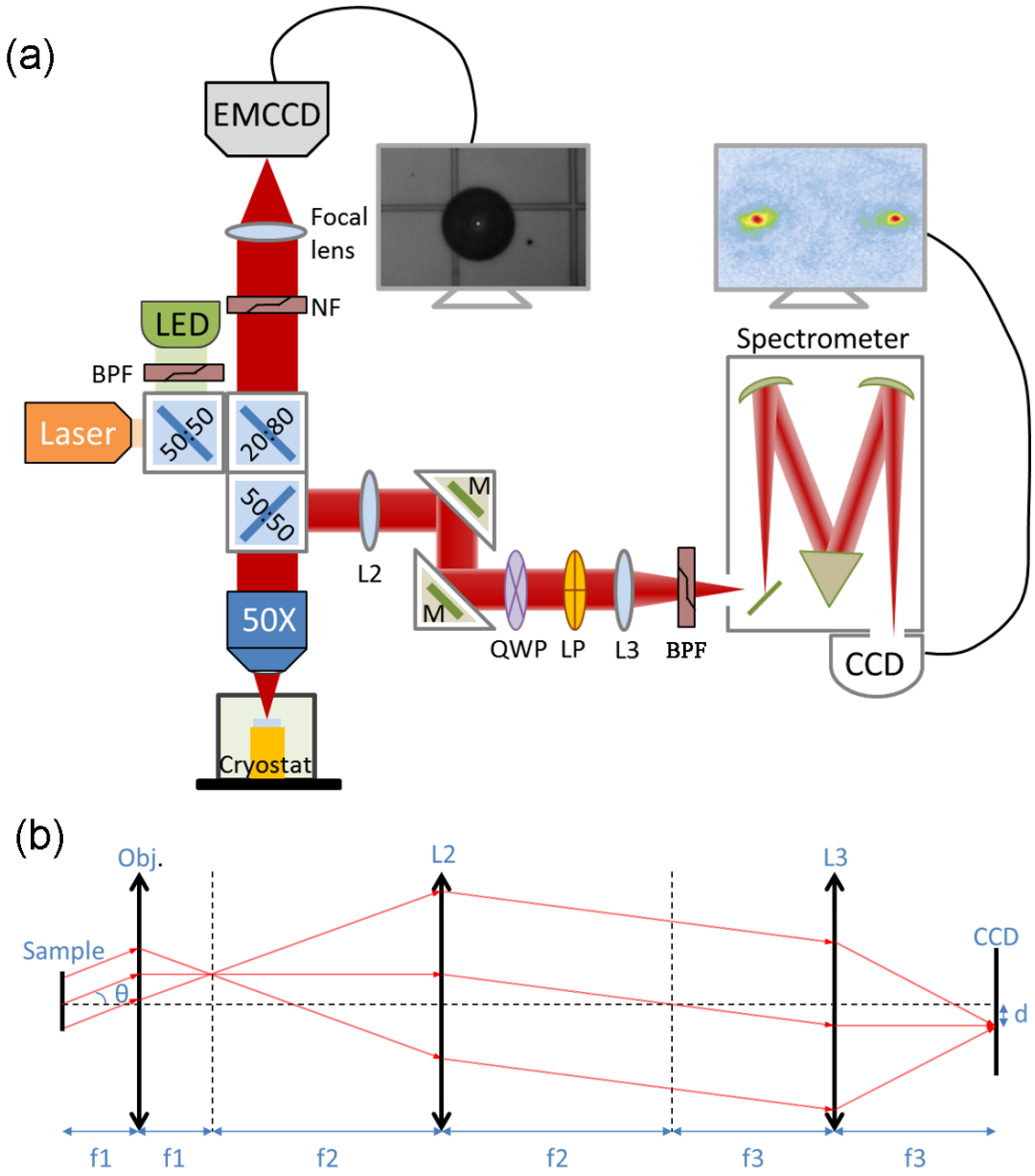

Fig. S7. Schematic of the optical setup for measuring the far-field scattering patterns. (a) A 785 nm continuous-wave laser is used to excite the photoluminescence (PL) of the InAs QD, which is then collected by a 50X objective (Olympus LCPLN50XIR) with NA=0.65. By inserting a lens ($f2$ = 400mm) between objective and another lens ($f3$=200mm) in front of the spectrometer (Princeton Instruments SP2750), the Fourier plane is imaged onto a CCD camera in order to measure the scattering angles of QD. In addition, a quarter-wave plate is used to switch the LCP and RCP into orthogonal linear polarization, followed by a linear polarizer to distinguish the LCP and RCP components of the QD emission. Optical components: mirror (M), banpass fliter (BPF), notch filter (NF), quarter waveplate (QWP) and linear polarizer (LP). (b) Schematic diagram of the conversion between the image size d and the scattered angles θ. The conversion between the CCD pixel and the scattered angles is calculated by $\frac{f1*tan\theta}{f2} =$

$\frac{d}{f3}$, where θ is the angle of emission light from sample; d represents the image size, that is equal to number of image pixel times pixel size (20 μm); $f1$, $f2$ and $f3$ are, respectively, the focal length of objective and two lenses (L2 and L3). $= 3.6\ mm$ is calculated from magnification of objective (50X) and its corresponding focal length of tube lens (180 mm).

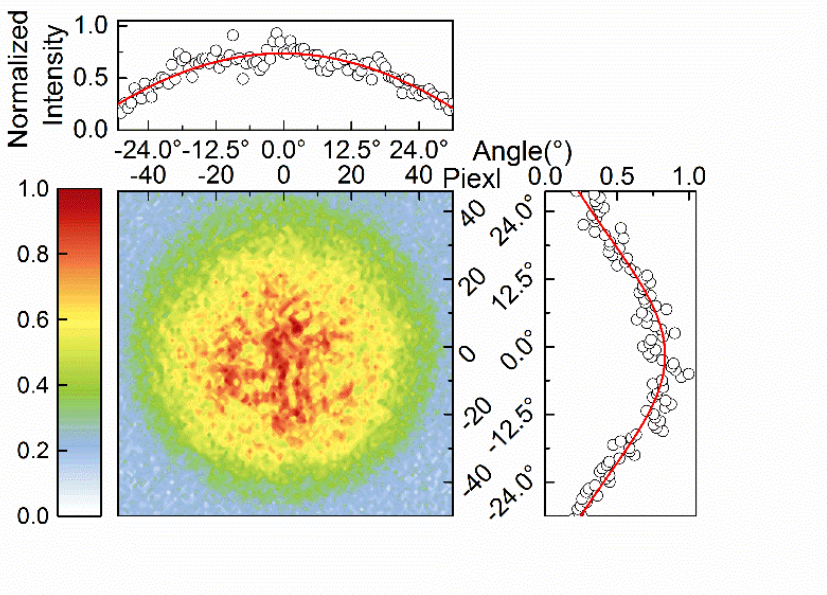

Fig. S8. Measured far-field scattering pattern of QD emission in a nanopillar structure without the top metasurface.

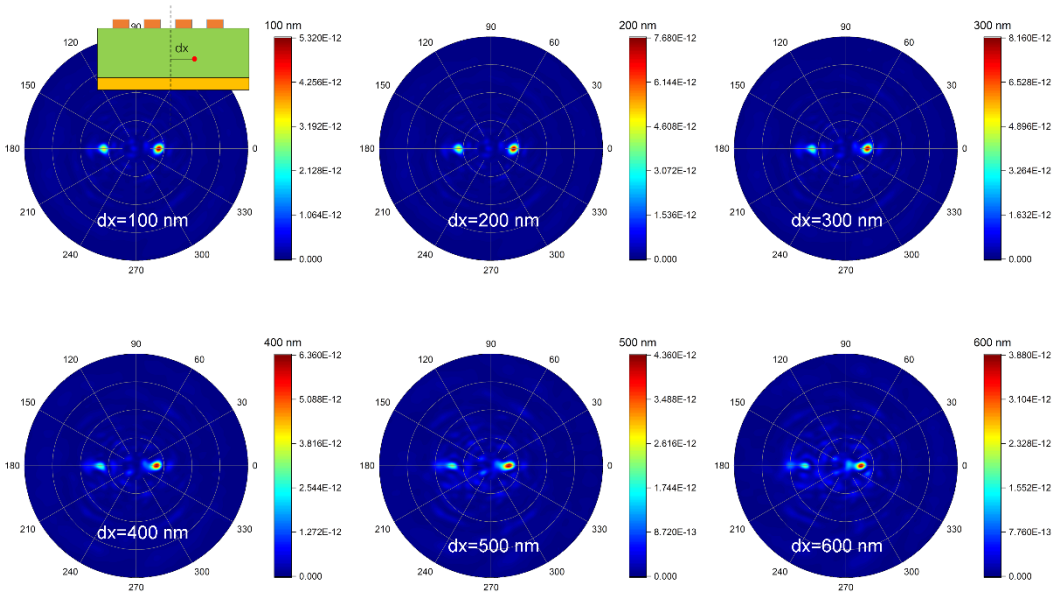

Fig. S9. Simulated far-field patterns of devices 2 with the QD position deviating from the center with a distance dx along x direction. With the position of the QD deviating from the center, the emission patterns become worse, and the emisson angles obviously deviate from the designed ones ±20°.

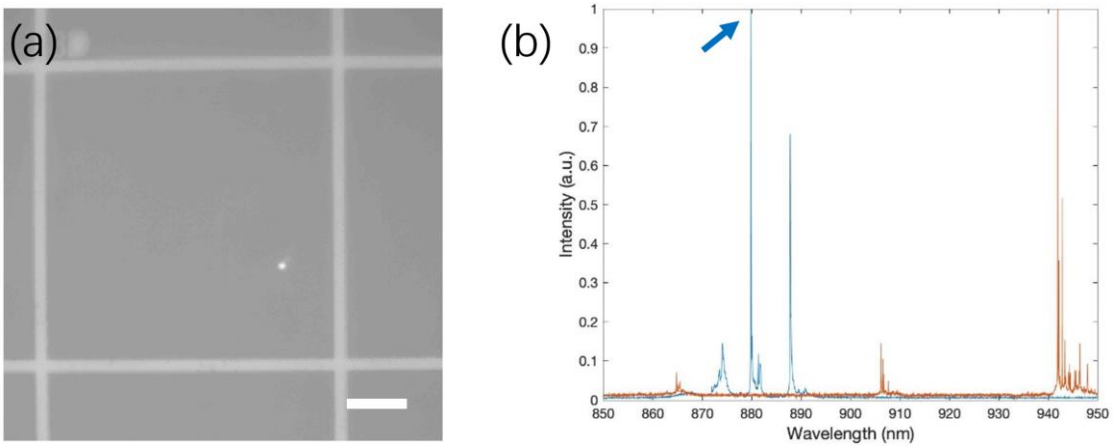

Fig. S10. The optical properties of the QDs. (a) The images of QDs together with gold markers are recorded by the fluorescence imaging technology. The white spot is the PL image from 1 QDs cluster and the size of the gold markers is 50 x 50 μm^2, which indicates the density of QDs is less than 1 QDs cluster per 50 x 50 μm^2. The scale bar is 10 μm. (b) The PL spectra of devices 1 (blue curve) and 2 (red curve), with most of the emission peaks of the QDs locating between 880 nm and 950 nm, i.e. the considering bandwidth in simulation. The blue arrow indicates the emission wavelength (879.903 nm) for second-order correlation function measurement.